Twenty-Seventh Symposium (International) on Combustion/The Combustion Institute, 1998/pp. 2335–2341

TRANSIENT COMBUSTION RESPONSE OF HOMOGENEOUS SOLID PROPELLANT TO ACOUSTIC OSCILLATIONS IN A ROCKET MOTOR

TAE-SEONG ROH, SOURABH APTE AND VIGOR YANG
The Pennsylvania State University
University Park, PA 16802, USA

Interactions between acoustic waves and the transient combustion response of a double-base homogeneous propellant in a rocket motor have been analyzed numerically. The analysis extends the previous work on gas-phase flame dynamics to include the coupling with condensed-phase processes. Consequently, a more complete description of propellant combustion response to imposed acoustic oscillations can be obtained. Emphasis is placed on the near-surface flame-zone physiochemistry and its coupling with unsteady propellant burning in an oscillatory environment. The formulation treats complete conservation equations and the finite-rate chemical kinetics in both the gas-phase and subsurface regions. The instantaneous propellant burning rate is predicted as part of the solution. Various distinct features of unsteady heat release arising from propellant combustion response in a motor with forced oscillations are studied systematically. As in the pure gas-phase dynamics of the previous case, the dynamic behavior of the luminous flame plays a decisive role in determining the motor stability characteristics. However, the propellant combustion response may qualitatively modify the temporal evolution of heat-release distribution in the luminous flame and as a result exerts a significant influence on the global stability behavior. The primary flame structure adjacent to the propellant surface is usually little affected by flow oscillation. This may be attributed to the large thermal inertia of the condensed phase, which tends to restrain the temperature variation in the near-surface zone in the present study of laminar flows. The situation with a turbulent flow may be drastically different, as turbulence may penetrate directly into the primary flame and substantially change the local flame dynamics and transport phenomena.

Introduction

This paper is a companion to our earlier work on the gas-phase combustion response of a double-base homogeneous propellant in a rocket motor [1]. The previous analysis mainly concentrated on the gas-phase flame dynamics and its response to acoustic oscillations. Detailed flow structures and heat-release mechanisms in various parts of the motor, including microscale motions in the near-surface flame zone and macroscale motions in the bulk of the chamber, were examined in depth. Strong interactions between exothermic reactions and acoustic waves were observed to take place in regions with steep temperature gradients, due to the large activation energy of the associated chemical kinetics. The dynamic behavior of the luminous flame played an important role in determining the motor stability characteristics in a laminar flow environment.

The present study extends the earlier gas-phase analysis to include the coupling with condensed-phase processes. Special attention is given to the interactions between near-surface flame-zone physiochemistry and subsurface pyrolysis. The model is based on complete conservation equations and finite-rate chemical reactions in both the gas and condensed phases. The instantaneous propellant burning rate is treated as part of the solution. Various underlying mechanisms responsible for driving unsteady motions in a motor, such as flame dynamics and propellant combustion response, are studied systematically to provide more insight into the problem. In order to avoid complications arising from turbulence, only laminar flows are considered here. A comprehensive analysis of laminar and turbulent flows will be performed in subsequent publications. Much experimental and numerical work has been performed on cold-flow simulations [2,3]. Recent studies by Vuillot et al. [4] and Cai and Yang [5] focussed on the two-phase flow in an oscillatory motor environment, but no attempt was made to calculate nonsteady propellant combustion characteristics in coupled gas and condensed-phase processes.

The present analysis has been carefully validated in every aspect against analytical solutions for cold-flow, propellant burning rates over a broad range of pressure and cross-flow conditions and pressure-coupled combustion response [1]. The work appears to be the first of its kind in treating detailed flow development and propellant combustion in a motor with forced oscillations. It represents a major step toward a comprehensive understanding of combustion instabilities of homogeneous propellants in rocket propulsion systems.

In subsequent sections, a theoretical formulation

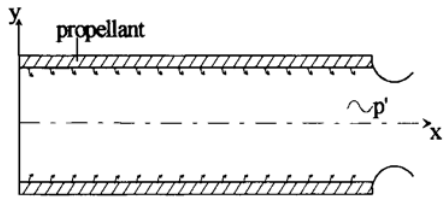

FIG. 1. Schematic diagram of a solid rocket motor.

of gas- and condensed-phase processes is briefly summarized, and the interfacial boundary conditions and their implementation are described. The analysis starts with calculations of the motor internal flow fields and propellant burning behavior under steady operating conditions. Periodic oscillations are then imposed at the exit to simulate standing acoustic waves in the chamber. The mutual coupling between unsteady heat release and local flow fluctuations, as well as their global effects on motor instability, are investigated in depth.

Theoretical Formulation

Gas-Phase Process

Figure 1 shows the physical model considered herein, a two-dimensional rocket motor loaded with double-base homogeneous propellant grains. Major ingredients of the propellant are 52% NC, 43% NG, and 5% additives. The formulation of the gas-phase process is identical to that established in Ref. [1]. In vector form, the governing equations for a multicomponent chemically reacting system of N species can be expressed as

$$\frac{\partial \mathbf{Q}}{\partial t} + \frac{\partial}{\partial x}(\mathbf{E} - \mathbf{E}_\mathbf{v}) + \frac{\partial}{\partial y}(\mathbf{F} - \mathbf{F}_\mathbf{v}) = \mathbf{S} \quad (1)$$

where x and y represent the axial and vertical coordinates, respectively. The conserved variable vector $\mathbf{Q}$ is

$$\mathbf{Q} = [\rho,\ \rho u,\ \rho v,\ \rho e,\ \rho Y_i]^T \quad (2)$$

The convective-flux vectors $\mathbf{E}$ and $\mathbf{F}$ and diffusion-flux vectors $\mathbf{E}_\mathbf{v}$ and $\mathbf{F}_\mathbf{v}$ follow the definitions given in Ref. [1]. A reduced chemical kinetics mechanism comprising two global reactions in the condensed phase and five reactions in the gas phase is employed to describe the combustion-wave structure [1].

Condensed-Phase Process

The condensed phase consists of a preheated zone and a superficial degradation (i.e., pyrolysis) layer in which molecular degradation of the propellant and reactions of the decomposed species take place. If we ignore bulk motion, mass diffusion, and axial thermal diffusion, and assume constant thermophysical properties, the formulation governing condensed-phase processes reduces to a set of one-dimensional equations [1]:
mass

$$\dot{m} = \rho_c r_b \quad (3)$$

energy

$$\rho_c C_c \frac{\partial T}{\partial t} + \dot{m} C_c \frac{\partial T}{\partial y} = \lambda_c \frac{\partial^2 T}{\partial y^2} + \dot{q}_c \quad (4)$$

species concentration

$$\rho_c \frac{\partial Y_i}{\partial t} + \dot{m} \frac{\partial Y_i}{\partial y} = \dot{\omega}_i \quad (5)$$

where ρ_c denotes propellant density and r_b burning rate. The rate of heat release per unit volume $\dot{q}_c$ is determined by the net effect of the endothermic decomposition and the exothermic reaction in the condensed phase. The in-depth boundary conditions associated with equations 4 and 5 are $T = T_i$ and $Y_p = 1$, respectively, where T_i is the initial (conditioned) temperature of the propellant. The surface conditions require that the propellant decomposition be completed; that is, $Y_p = 0$ and $T = T_s$.

Interfacial Conditions

The processes in the gas and condensed phases are matched at the propellant surface by requiring continuities of mass and energy. This procedure eventually determines the propellant burning rate and surface temperature and species concentrations.

With the application of conservation laws to the gas–solid interface, the matching conditions are expressed as follows [1]:
mass balance for mixture

$$(\rho v)_g = -\rho_c r_b \quad (6)$$

mass balance for species i

$$[\rho(v + \hat{v}_i)Y_i]_g = -\rho_c r_b Y_{i,s} \quad (7)$$

energy balance

$$-\lambda_g \left(\frac{\partial T}{\partial y}\right)_g + \left[\rho \sum_{i=1}^{N} Y_i h_i (v + \hat{v}_i)\right]_g = -\lambda_c \left(\frac{\partial T}{\partial y}\right)_s - \rho_c r_b \times \left[C_c(T_s - T_{ref}) + \sum_{i=1}^{N} Y_i h_{f,i}^o\right]_s \quad (8)$$

Subscripts g and s represent conditions at the interface on the gas and solid sides, respectively. Since molecular degradation takes place in an exceedingly

thin layer, on the order of a few microns, the corresponding residence time is much shorter than that in the preheated zone by at least 1 order of magnitude [6]. A quasi-steady-state approximation is therefore employed in determining the subsurface pyrolysis behavior. The net heat flux to the preheated zone can be obtained by integrating the energy equation for the superficial degradation layer [7,8].

$$\lambda_c \left(\frac{\partial T}{\partial y}\right)_c = \lambda_g \left(\frac{\partial T}{\partial y}\right)_g + \dot{m}[\bar{Q}_s + (C_c - C_p)(T_s - \bar{T}_s)] \quad (9)$$

where $\bar{Q}_s$ and $\bar{T}_s$ are the net subsurface heat release and surface temperature under steady-state conditions, respectively. A matched asymptotic expansion technique similar to that derived in Refs. [9,10] is established to relate the propellant burning rate to the local heat fluxes across the superficial degradation layer:

$$r_b^o = \frac{\alpha_c A_c \exp(-\beta)/\beta}{\left\{(\lambda_g/\dot{m})\left(\frac{\partial T}{\partial y}\right)_g + [\bar{Q}_s + (C_c - C_p)(T_s - \bar{T}_s)]/2\right\}/(C_c T_s)} \quad (10)$$

This equation, along with equations 6, 7, and 9, is sufficient to solve for the propellant burning rate and the set of unknowns (v, T, Y_i) at the propellant surface.

Boundary Conditions

Boundary conditions at the exit must be carefully treated based on the method of characteristics to avoid spurious, nonphysical acoustic reflections. Because the outflow is subsonic, only one physical condition needs to be specified. The remaining conditions can be obtained by appropriately manipulating the governing and characteristic equations, as suggested by Watson and Myers [11]. At the upstream boundary, the axial velocity and the gradients of pressure and radial velocity are set to zero along the solid wall to prevent the occurrence of a numerically produced recirculating flow near the head end. Finally, flow symmetry is assumed at the centerline.

Numerical Method

A time-accurate scheme based on a dual time-stepping integration method is used in the present work [12]. The algorithm employs pressure decomposition and preconditioning techniques to circumvent numerical difficulties encountered for low Mach number flows in rocket motor environments. Further efficiency is obtained by implementing a fully coupled implicit ADI scheme. The present formulation renders the numerical method very stable and robust and allows the selection of the time step to be dictated by physical processes. The solution to the gas phase is obtained first, and then an iterative method is used to determine the propellant mass burning rate and temperature distribution in the condensed phase at each physical time step. The temperature, species composition, and mass burning rate at the interface thus obtained are taken as the initial conditions for the gas-phase analysis. The condensed and gas-phase calculations proceed in turn, overlapping each other by one-half of the physical time step.

Results and Discussion

The interactions between gas-phase flame dynamics and condensed-phase response in standing acoustic-wave environments have been studied using the analysis described earlier. The propellant ingredients, chamber dimensions, and operating conditions are identical to those in Ref. [1]. The computational domain for the condensed phase measures 100 μm in depth, which is about twice the estimated thickness of the preheated zone at 60 bar. The corresponding numerical grid consists of 80 and 50 points in the axial and vertical directions, respectively, and is clustered near the burning surface to resolve the steep gradients of temperature and species concentrations there. The smallest grid spacing normal to the surface is about 0.1 μm. After the steady-state flow field is obtained, periodic oscillations of frequencies of 877.5 and 1755.1 Hz are imposed at the chamber exit to simulate longitudinal standing waves of the first and second modes, respectively. The amplitude of the oscillation is 2% of the mean pressure. Data analysis of unsteady flow characteristics is conducted after steady oscillations are achieved in the eighth cycle of the imposed acoustic oscillations.

Pressure and Velocity Fields

As in the previous case of pure gas-phase dynamics without any condensed-phase coupling [1], the acoustic pressure field is basically one dimensional. No discernible variation in the vertical direction is observed, due to the low Mach number environment under consideration. The oscillatory velocity field, however, exhibits a complex multidimensional structure adjacent to the burning surface within which rapid variations arising from the interactions between acoustic disturbances, unsteady shear waves, and flame oscillations occur. Figures 2a and 2b present the results of the first and second modes, respectively. Only the upper portion of the chamber is covered to provide better resolution of the flow field. The existence of an acoustic boundary layer is clearly

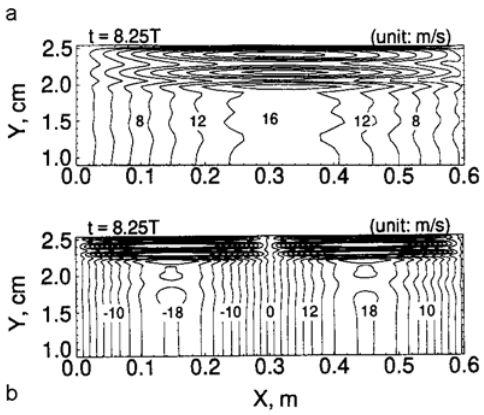

FIG. 2. Contour plots of axial velocity fluctuation: (*a*) first mode and (*b*) second mode.

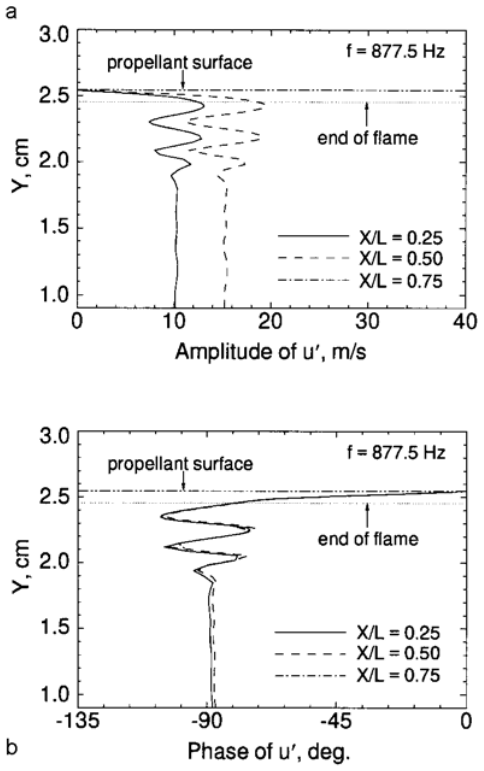

FIG. 3. Vertical distributions of axial velocity fluctuation of first mode at various locations: (*a*) amplitude and (*b*) phase.

observed. The primary difference between the two modes lies in the spatial structure and phase distribution of the oscillatory field. The thickness of the acoustic boundary layer decreases with increasing frequency due to enhanced viscous damping. Figures 3a and 3b show the vertical distributions of the amplitude and phase of the axial velocity fluctuation u' of the first mode at three axial locations, respectively. Also included is the flame thickness defined by the location at which the temperature reaches 97% of the final flame temperature. Compared with the cold-flow simulation in which chemical reactions are not involved [13], the rapid increase of temperature in the flame zone tends to suppress the growth of velocity fluctuation, due to the strong variation of acoustic impedance [14]. In the core region, where the shear wave diminishes, the velocity fluctuation follows the isentropic relation with the acoustic pressure, with a phase lag of 90° with reference to p'. The amplitude of u' reaches a magnitude of 14.14 m/s at the acoustic pressure node point ($x/L = 0.5$).

The distribution of vertical velocity fluctuations v' for the first mode (figure not shown) bears a strong resemblance to the earlier case for pure gas-phase dynamics [1]. The transient combustion response of the propellant only renders a slight increase of v' at the surface. A simple analysis based on the calculated mass burning-rate fluctuation yields a value of v' at the surface around 5 mm/s. This velocity fluctuation is too low to exert any significant influence on flame structure as compared with the situation with no condensed-phase coupling but is sufficient to modify the global stability behavior through its effect on the time evolution of heat-release distributions, a phenomenon discussed later.

Temperature Field and Heat-Release Distribution

The temporal evolution of the temperature field and its associated heat-release distribution was obtained to provide direct insight into the oscillatory combustion mechanisms. A large temperature oscillation occurs in the luminous flame zone where the major heat-release mechanism is associated with the reduction of NO species. The large activation energy of the NO reaction produces a stiff flame with a steep temperature gradient, and as such, any small variation of the flame location due to local flow disturbances may cause a substantial oscillation of the temperature field. Also noteworthy is the small perturbation of the propellant surface temperature, about 1 K in the present study. The large thermal inertia in the condensed phase tends to restrain the temperature disturbance near the surface, with the primary flame being practically unaffected. It should be noted that this observation is valid only for laminar flows. The situation in a turbulent flow environment may be considerably different, since turbulence may penetrate into the primary flame and

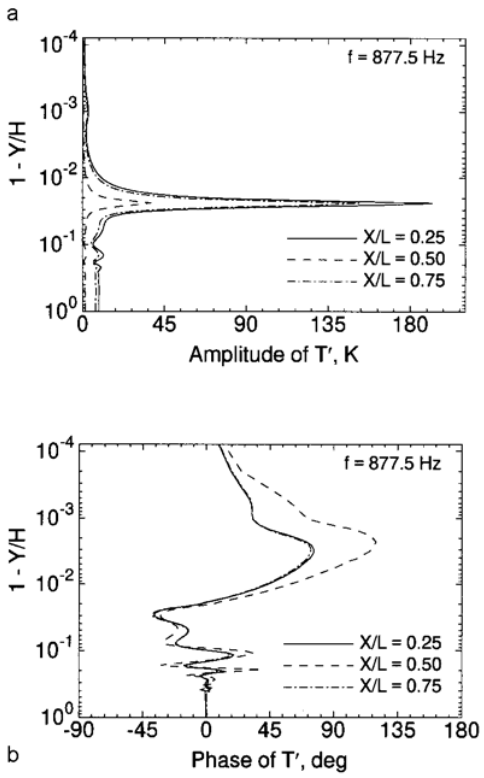

FIG. 4. Vertical distributions of temperature fluctuation of first mode at various axial locations: (*a*) amplitude and (*b*) phase.

qualitatively modify the local flame dynamics and its coupling with the propellant response [15,16].

Figures 4a and 4b present the vertical distributions of the amplitude and phase of temperature fluctuation for the first mode. Although the amplitude shows the same behavior as observed in Ref. [1], the phase distribution becomes quite different due to the transient response of the condensed phase. A large phase variation is observed in the entire flame zone and consequently leads to a qualitative change in the heat-release characteristics. The maximum temperature variation in the core-flow region is about 10 K, following the isentropic relation with the acoustic pressure, because this region has no chemical reaction and negligibly small viscous stress. The vertical distribution of the heat-release fluctuation is shown in Fig. 5. It basically follows the gradient of the temperature fluctuation, easily explained by the energy balance over a control volume [1]. The distribution exhibits two peak values with a phase difference of around 180° between them in the luminous flame zone, a phenomenon commonly observed for flames with steep temperature profiles.

One critical issue in the present study is the transient combustion response of the propellant to local flow oscillations in a rocket motor environment. In this regard, calculations were made to determine the fluctuations of propellant surface temperature and mass burning rate, yielding the results shown in Fig. 6. Of particular interest is that the mass burning-rate fluctuation uniformly lags the pressure fluctuation by about 20° along the entire propellant surface. The propellant combustion response is basically pressure dominant, and the velocity-coupling effect appears to be subdued in the present study of laminar flows. The calculated combustion response function, $R_P = [(\dot{m}'/\bar{\dot{m}})]/(p'/\bar{p})$ has a real part of 1.72 and an imaginary part of 1.53, being in good agreement with the experimental data obtained by Lengelle et al. [17].

Instantaneous contour plots of condensed-phase temperature fluctuation for the first and second modes are shown in Figs. 7a and 7b, respectively. The distributions follow a pattern corresponding to the standing acoustic-wave structure in the gas phase. The temperature fluctuation reaches its maximum value at the pressure antinode point and vanishes at the node points, further confirming the predominance of pressure-coupled combustion response. The maximum surface-temperature fluctuations are 1.2 and 1.6 K for the first and second modes, respectively. The penetration depth of the thermal wave δ_p decreases with increasing frequency and can be estimated using a simple dimensional analysis, $\delta_p = \sqrt{\alpha_p/f}$, where α_p stands for the thermal diffusivity of propellant.

Rayleigh's Parameter

The unsteady heat release needs to be correlated with the acoustic pressure to provide a quantitative measure of the extent to which the flame may drive or suppress flow oscillations in the chamber. This can be easily achieved by calculating the Rayleigh parameter, $\langle p'q' \rangle$, a time-averaged quantity of the product of acoustic pressure and heat-release fluctuation over one cycle of oscillation. In the previous work on pure gas-phase dynamics [1], two positive peaks associated with the oscillation of the luminous flame were obtained in the vertical distribution of Rayleigh's parameter for the first mode, suggesting that the oscillatory flame serves as a combination of an acoustic monopole and a dipole source for driving instabilities in the chamber. The situation is drastically changed in the present study, as shown in Fig. 8, for the first mode. The transient response of the condensed phase may substantially modify the time evolution of local heat release, in spite of its limited effect on the magnitude of heat release [18]. Consequently, the distribution of Rayleigh's parameter exhibits both a positive and a negative peak having

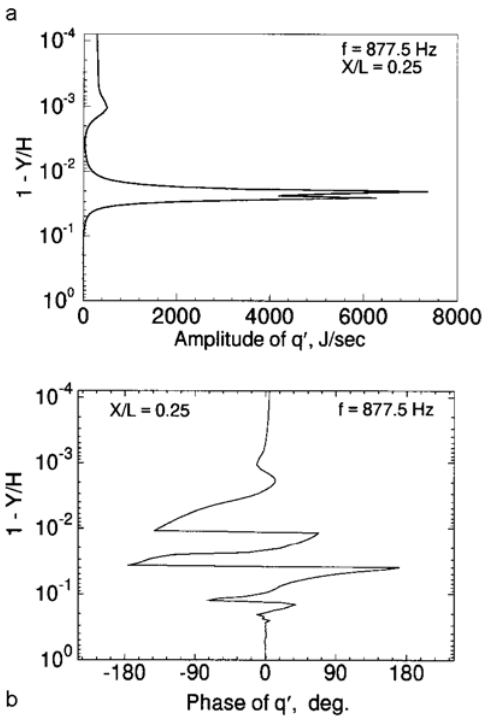

FIG. 5. Vertical distributions of heat-release fluctuation of first mode at $x/L = 0.25$: (*a*) amplitude and (*b*) phase.

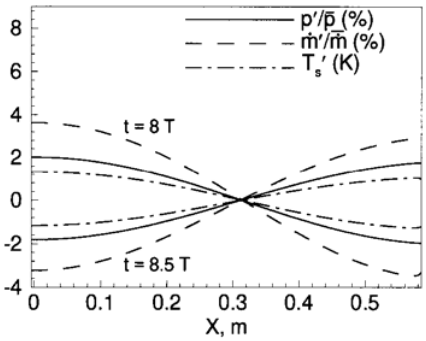

FIG. 6. Instantaneous distributions of pressure, mass burning rate, and surface-temperature fluctuations.

about the same amplitude. The luminous flame behaves as an acoustic dipole source. The structure of the second mode is even more complicated (not shown). For both modes, the net value of $\langle p'q' \rangle$ is positive. The unsteady heat release resulting from the flame response to acoustic fluctuations tends to excite flow oscillations in the chamber.

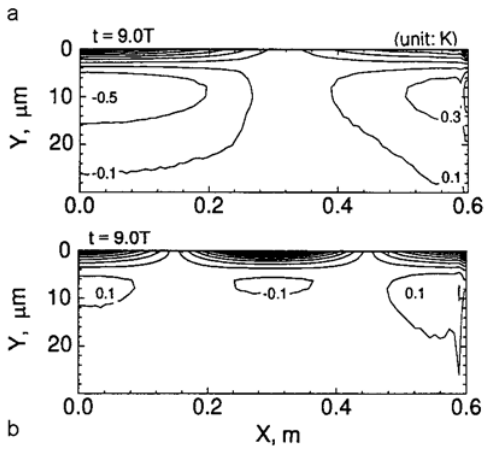

FIG. 7. Contour plots of temperature fluctuation in condensed phase: (*a*) first mode and (*b*) second mode.

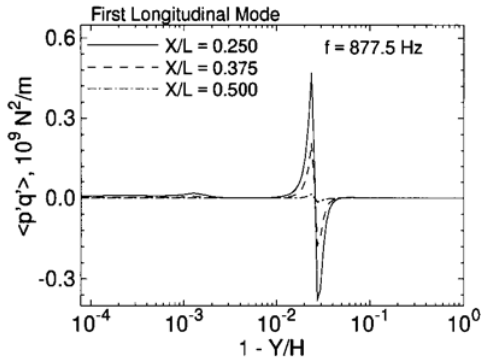

FIG. 8. Vertical distributions of Rayleigh's parameter at various axial locations for first mode.

Conclusion

The transient combustion response of a double-base homogeneous solid propellant to acoustic waves in a rocket motor with forced oscillations has been investigated in detail. Compared with the previously studied case for pure gas-phase dynamics, the acoustic velocity field remains basically unchanged except for a slight modification of the vertical velocity fluctuation near the burning surface. The condensed-phase response may, however, substantially change the temporal evolution of the temperature and heat-release distributions in the luminous flame zone and consequently may modify the global stability characteristics of the motor in terms of Rayleigh's parameter. The primary flame structure is little affected in the present study of laminar flows, even with the condensed-phase coupling. This may

be attributed to the large thermal interia in the condensed phase, which effectively restrains temperature perturbations in the near surface zone. The situation with turbulent flows may be drastically different due to turbulence-enhanced transport in the flame zone. Future studies on propellant combustion response in motor environments must address this issue.

Nomenclature

C_p specific heat of gas
C_c specific heat of condensed phase
e specific total internal energy
$\mathbf{F}$ convective flux vector
$\mathbf{F_v}$ diffusion flux vector
E_i activation energy
h_i specific enthalpy of species i
$h^o_{f,i}$ heat of formation of species i
$\dot{m}$ mass burning rate
p pressure
$\dot{q}_c$ rate of heat release in condensed phase per unit volume
q thermal diffusion term
$\mathbf{Q}$ dependent variable vector
Q_i heat release from reaction of species i
Q_c total heat release in condensed phase
r_b propellant burning rate
$\mathbf{S}$ source vector
t time
T temperature or period of oscillation
v velocity
$\hat{v}_i$ diffusion velocities of gas-phase species i
$\bar{W}$ molecular weight of mixture
y Cartesian coordinate
Y_i mass fraction of species i

Greek Symbols

β normalized activation energy
λ thermal conductivity or wavelength
ρ density
τ viscous stress
$\dot{\omega}_i$ rate of production of species i

Subscript

c condensed phase
f gas-phase flame
g gas phase
i ith species or initial condition
p propellant
s burning surface

Superscript

T transpose of vector
$'$ fluctuating quantity

REFERENCES

1. Roh, T. S., Tseng, I. S., and Yang, V., *J. Propul. Power* 11:2241–2255 (1995).
2. Vuillot, F., *J. Propul. Power* 11:626–639 (1995).
3. Kourta, A., *J. Propul. Power* 2:371–376 (1996).
4. Vuillot, F., Dupays, J., and Lupoglazoff, N., AIAA paper 97-3326, 1997.
5. Cai, W. D. and Yang, V., AIAA paper 98-0161, 1998.
6. Zenin, A. A., *Combust. Explos. Shock Waves* 2:67–76 (1966).
7. Levine, J. N. and Culick, F. E. C., "Nonlinear Analysis of Solid Rocket Combustion Instability," AFRPL-TR-74-45, October, 1974.
8. Kooker, D. E. and Nelson, C. W., "Numerical Solution of Solid Propellant Transient Combustion," AIChE-ASME Heat Transfer Conference, August, 1978.
9. Lengelle, G., *AIAA J.* 8:1989–1996 (1970).
10. Ibiricu, M. M. and Williams, F. A., *Combust. Flame* 24:185–198 (1975).
11. Watson, W. R. and Myers, M. K., *AIAA J.* 29:1383–1389 (1991).
12. Hsieh, S. Y. and Yang, V., *J. Comp. Fluid Dyn.* 8:31–49 (1997).
13. Flandro, G. A., *J. Propul. Power* 11:607–625 (1995).
14. Tseng, C. F., Chu, W. W., and Yang, V., *Combust. Flame,* in press (1998).
15. Tseng, C. H. and Yang, V., *Combust. Flame* 96:325–342 (1994).
16. Roh, T. S. and Yang, V., AIAA paper 96-2663, 1996.
17. Lengelle, G., Bizot, A., Duterque, J., and Trubert, J. F., "Solid Propellant Steady State Combustion: Physical Aspects," AGARD Lecture Series 180, 1991.
18. Roh, T. S., "Numerical Simulation of Combustion Instabilities of Double-Base Homogeneous Propellant in Rocket Motors," Ph.D. thesis, Pennsylvania State University, University Park, 1995.